Available online at www.sciencedirect.com
SCIENCE DIRECT®
ELSEVIER
International Journal of Multiphase Flow 30 (2004) 67–87
International Journal of Multiphase Flow
www.elsevier.com/locate/ijmulflow

Flocculation in simulations of sheared fiber suspensions

Leonard H. Switzer *, Daniel J. Klingenberg

Department of Chemical Engineering and Rheology Research Center, University of Wisconsin, Madison, WI, USA

Received 26 September 2002; received in revised form 28 October 2003

Abstract

We have developed a particle-level, dynamic simulation technique to probe the structural behavior of non-Brownian fiber suspensions in simple shear flow. The model incorporates a variety of realistic features including fiber flexibility, irregular equilibrium fiber shapes, and fiber interactions. Simulated suspensions exhibit heterogeneous structures, or flocculation, when the model fibers are flexible, have deformed equilibrium shapes, and interact through static friction forces, even in the absence of attractive forces between fibers. The addition of kinetic friction and weak attractive forces has little effect on flocculation behavior, while anisotropic fiber bending tends to shift the onset of flocculation to larger coefficients of friction.

Keywords: Flocculation; Flexible fibers; Simulation; Fiber suspensions

1. Introduction

Suspensions of non-Brownian fibers are found in a variety of applications, such as pulp and paper and fiber-filled composites processing. The physical characteristics of the suspensions, as well as the properties of the final products, depend on the structure of the suspensions. The structure is affected by such features as the fiber properties, interactions, and flow fields. Understanding the relationships among these features, the suspension structure, and the macroscopic properties can therefore aid in the design and optimization of processes and products. In this article, we employ a fiber-level simulation method to probe the relationships between fiber properties, interactions, and the suspension structure.

Many applications require a homogeneous suspensions of fiber to yield uniform products. Long flexible fibers, however, tend to aggregate, forming spatially heterogeneous structures. The formation of such heterogeneous distributions of mass is commonly referred to as "flocculation," and the fibrous aggregates are referred to as "flocs" (Mason, 1950; Kerekes et al., 1985; Soszynski

* Corresponding author.

0301-9322/$ - see front matter © 2003 Published by Elsevier Ltd.
doi:10.1016/j.ijmultiphaseflow.2003.10.005

and Kerekes, 1988a,b; Kerekes and Schell, 1992). Such structures are undesirable in papermaking, leading to poor paper quality (Mason, 1950; Robertson, 1956; Kerekes and Schell, 1992).

While aggregation in colloidal dispersions typically arises from attractive interparticle forces (Russel et al., 1989), Mason (1948, 1950) suggested that non-Brownian fibers can aggregate by a mechanical mechanism. Fibers in shear flow translate and rotate, resulting in collisions between fibers. Above a critical concentration ($nL^3 \gtrsim 1$, where n is the fiber number density and L is the fiber length), the frequent forced collisions between fibers can lead to flocculation via mechanical entanglement. Meyer and Wahren (1964) and Soszynski and Kerekes (1988a,b) expanded on this notion, proposing a more detailed picture of the flocculation process. Flexible fibers in a flow with non-zero velocity gradients will be exposed to viscous and dynamic forces (Meyer and Wahren, 1964), as well as interfiber contact forces (Soszynski and Kerekes, 1988a,b), which elastically deform the fibers. When the flow ceases, the fibers attempt to relax, but if the concentration is sufficiently large, the fibers will contact other fibers and come to rest in elastically strained configurations. The result is a mechanically coherent fiber network or floc. Soszynski and Kerekes (1988a) provided evidence for this mechanism by conducting experiments with suspensions of nylon fibers. Suspensions subjected to flow in a rotating, half-filled cylinder formed coherent fiber flocs above a critical concentration. These flocs possessed sufficient mechanical strength to be manually extracted from the cylinder. Some of these flocs were heated above the glass transition temperature of nylon to relax the stored elastic stresses within the fibers, and then cooled to room temperature. The heat-treated flocs dispersed easily under gentle stirring, while the never-heated flocs only dispersed under intense stirring. The authors called this mechanism of flocculation "interlocking by the elastic bending of fibers." While other forces, such as colloidal forces and interfacial tension arising from entrained gas bubbles, can certainly contribute to fiber aggregation in some systems, it appears that the elastic-interlocking mechanism can contribute to flocculation in any sufficiently concentrated suspension of flexible fibers.

Meyer and Wahren (1964) modelled concentrated suspensions of flexible fibers as elastically interlocked networks, where each fiber is in contact with at least three others. The predicted dependence of the shear modulus on fiber aspect ratio $r_p = L/d$ (d is the fiber diameter), volume fraction Φ, and fiber Young's modulus E_Y agreed reasonably well with experimental data on pulp suspensions (Thalén and Wahren, 1964; Almin et al., 1967). Bennington et al. (1990) applied a similar network theory to describe their experimental data on the yield stress of suspensions of synthetic and wood fibers. The predicted dependence of the yield stress on fiber aspect ratio and volume fraction agreed fairly well with experimental results. However, the predicted dependence on the fiber elastic modulus did not agree well with experiments, particularly for the wood fibers. The authors attributed the lack of agreement to more complex surface interactions than that accounted for in the model. It is also possible that, contrary to the assumption in the network theory, the structure of the network may depend on the fiber modulus, and thus the predicted simple dependence of the network properties on fiber modulus may not hold. Indeed, the flocculation behavior of suspensions and thus their microstructure depends on numerous variables, including the suspending fluid viscosity (Zhao and Kerekes, 1993), the deformation rate (Takeuchi et al., 1983; Hourani, 1988), the fiber length (Soszynski and Kerekes, 1988a,b; Kerekes and Schell, 1995), the concentration (Kerekes and Schell, 1992), and the type and amount of additives (Zauscher et al., 2000; Beghello, 1998). We will show in this article that the structure predicted by simulations also depends on the fiber modulus.

Particle-level simulations are common methods for probing particulate suspensions, and more specifically, for understanding the relationships between particle properties and interactions, the suspension structure, and macroscopic behavior (see, for example, Bossis and Brady, 1987). The equations of motion for each particle are solved numerically, subject to the forces and torques identified, in order to evolve the particle positions and orientations in time, and thus produce a prediction of the suspension microstructure. This method is sufficiently general to allow the inclusion of a variety of features, such as elongated and flexible particles, as well as various forces, such as hydrodynamic forces and interactions, colloidal forces and friction, to name a few. The complexity of the physical model is only limited by the computational resources required to evaluate the forces and torques and solve the equations of motion.

Numerous fiber suspension studies have focused on rigid, elongated bodies in Newtonian fluids. Claeys and Brady (1993a,b) modelled fibers as rigid prolate spheroids (ellipsoids of revolution). They developed a method for accurately evaluating the hydrodynamic forces and torques, including both short-range hydrodynamic interactions (lubrication forces) as well as long-range, many-body hydrodynamic interactions. Mackaplow and Shaqfeh (1996) employed slender-body theory to accurately evaluate the long-range hydrodynamic interactions between prolate spheroids or cylinders. As with the method of Claeys and Brady, the calculations were so computationally demanding that results for suspensions of long fibers in simple shear flow were limited to prescribed suspension structures. Thus these methods were not employed to predict the suspension structure resulting from flow. Simulations by Yamane et al. (1994) and Fan et al. (1998) employed approximations for the hydrodynamic interactions between rigid fibers. These authors did not report fiber flocculation under the conditions simulated ($nL^3 \lesssim 50$, $r_p \lesssim 30$).

Sundararajakumar and Koch (1997) and Harlen et al. (1999) simulated suspensions of rigid, slender rods interacting via contact forces. They argued that for flowing suspensions of fibers, lubrication forces cannot prevent fibers from contacting, and thus short-range hydrodynamic interactions were neglected. Harlen et al. (1999) simulated single spheres falling through neutrally buoyant fiber suspensions to illustrate the importance of fiber–fiber contacts on the flow properties of fiber suspensions. For low concentrations, interfiber contacts are rare and the flow behavior is dominated by long-range hydrodynamic interactions. However, as the concentration is increased such that the fibers are in frequent contact, the flow behavior is strongly influenced by the contacts. In fact, for $nL^3 \geqslant 12$ ($r_p = 20$), the drag on the settling sphere calculated by including long-range hydrodynamic interactions and contact forces is indistinguishable from that calculated by including contact forces alone (and in good agreement with experimental results reported by Milliken et al., 1989). Although the falling sphere influences the suspension structure, the authors did not report any tendency toward fiber flocculation.

Several studies have focused on simulating suspensions of flexible fibers. Yamamoto and Matsuoka (1993, 1994) modelled flexible fibers as chains of rigid spheres connected through springs, with potentials to mimic resistance to bending and twisting. Chain connectivity is maintained by constraints, producing equations that must be solved simultaneously with the equations of motion. Ross and Klingenberg (1997) modelled flexible fibers as inextensible chains of rigid prolate spheroids connected through ball and socket joints. This model eliminates the need for iterative constraints to maintain fiber connectivity, and can represent large aspect ratio fibers with relatively few bodies. These features help to reduce computations, facilitating simulation of concentrated suspensions. Schmid et al. (2000) extended this method, modelling flexible

fibers as chains of spherocylinders connected by ball and socket joints, that interacted via short-range repulsive forces as well as friction forces. While attractive forces can certainly give rise to fiber aggregation (Schmid and Klingenberg, 2000a), Schmid et al. (2000) demonstrated that interfiber friction—in the absence of attractive forces—can produce fiber flocculation.

In this article, we expand upon the study of Schmid et al. (2000) to probe flocculation in flexible fiber suspensions caused by friction forces. The fiber model and simulation method are briefly described in Section 2. In Section 3.1, we summarize the results obtained by Schmid et al., illustrating the importance of friction, fiber stiffness, and fiber shape on flocculation. Results from the present study are described in the subsequent sections, where the effects of friction, fiber stiffness and shape on flocculation are investigated further, and the influence of other fiber features are explored. In Section 3.2, we show that the coefficient of friction necessary to hold model flocs intact decreases with increasing fiber stiffness, and that friction-induced flocculation can occur for values of friction coefficients and fiber stiffnesses similar to those measured experimentally. We also illustrate how friction-induced flocculation is consistent with several experimental observations. The effects of fiber shape are probed in Section 3.3. The concentration at which U-shaped fibers flocculate decreases with increasing fiber curvature. We show that sliding friction (Section 3.4) and weak attractive forces (Section 3.5) have little impact on friction-induced flocculation. In Section 3.6, we show that, in some cases, anisotropic fiber bending can inhibit flocculation. Conclusions from this work are summarized in Section 4.

2. Simulation method

Flexible fiber suspensions are modelled as neutrally buoyant chains of linked rigid bodies immersed in a Newtonian liquid. The model includes realistic features such as fiber flexibility, irregular equilibrium shapes, and mechanical contact forces between fibers. The model and simulation method are similar to those employed by Schmid et al. (2000) and are described in more detail elsewhere (Switzer, 2002).

Each fiber in the suspension is represented by N_{seg} rigid cylinders (length 2ℓ, radius b) with hemi-spherical end caps, connected end-to-end by ball and socket joints (Fig. 1). The motion of

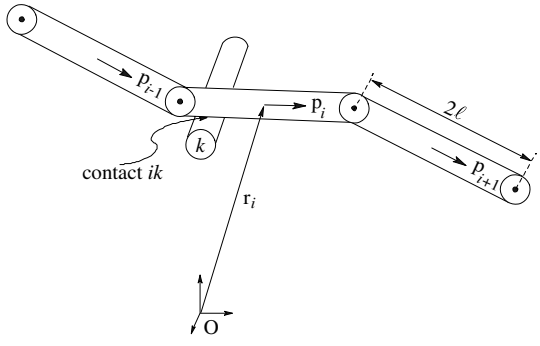

Fig. 1. Schematic diagram of a model fiber composed of rigid spherocylinders linked by ball and socket joints. Here, segment i is in contact with segment k from another fiber.

the fiber segments is described by Newton's laws of motion in which we neglect fiber inertia. The force balance on a fiber segment i includes contributions from hydrodynamic drag ($\mathbf{F}_i^{\mathrm{hyd}}$), mechanical contact forces ($\mathbf{F}_{ik}^{\mathrm{con}}$), and forces at each joint that maintain the segment connectivity ($\mathbf{X}_i$),

$$\mathbf{F}_i^{\mathrm{hyd}} + \mathbf{X}_{i+1} - \mathbf{X}_i + \sum_k^{N_{C_i}} \mathbf{F}_{ik}^{\mathrm{con}} = \mathbf{0}, \tag{1}$$

where N_{C_i} is the number of contacts on fiber segment i. The torque balance on fiber segment i includes similar contributions with the addition of a restoring torque at each joint ($\mathbf{Y}_i$),

$$\mathbf{T}_i^{\mathrm{hyd}} + \mathbf{Y}_{i+1} - \mathbf{Y}_i + \ell \mathbf{p}_i \times [\mathbf{X}_{i+1} + \mathbf{X}_i] + \sum_k^{N_{C_i}} \left[\mathbf{G}_{ik} \times \mathbf{F}_{ik}^{\mathrm{con}}\right] = \mathbf{0}, \tag{2}$$

where $\mathbf{T}_i^{\mathrm{hyd}}$ is the hydrodynamic torque, $\mathbf{p}_i$ is the orientation vector of the segment, and $\mathbf{G}_{ik}$ is a vector from the center of segment i to the point of contact with segment k.

In this model, hydrodynamic interactions are neglected based on simulations performed by Sundararajakumar and Koch (1997) and Harlen et al. (1999), as previously explained. This assumption allows us to evaluate the hydrodynamic drag force and torque as that on an isolated body, $\mathbf{F}_i^{\mathrm{hyd}} = \mathbf{A}_i \cdot [\mathbf{U}_i^{\infty} - \dot{\mathbf{r}}_i]$ and $\mathbf{T}_i^{\mathrm{hyd}} = \mathbf{C}_i \cdot [\mathbf{\Omega}_i^{\infty} - \boldsymbol{\omega}_i] + \widetilde{\mathbf{H}}_i : \mathbf{E}^{\infty}$, where the resistance tensors $\mathbf{A}_i$, $\mathbf{C}_i$, and $\widetilde{\mathbf{H}}_i$ for the spherocylinder segments are approximated by the resistance tensors of a prolate spheroid with an equivalent aspect ratio $r_e = 0.7 r_p / N_{seg}$ (Schmid et al., 2000; Switzer, 2002). The ambient velocity $\mathbf{U}_i^{\infty}$, angular velocity $\mathbf{\Omega}_i^{\infty}$, and rate of strain tensor $\mathbf{E}^{\infty}$ are evaluated at the center of mass of each segment, and only simple shear flows are simulated (i.e., $\mathbf{U}^{\infty} = (\dot{\gamma} z, 0, 0)$, where $\dot{\gamma}$ is the shear rate). The segment translational and angular velocities are $\dot{\mathbf{r}}_i$ and $\boldsymbol{\omega}_i$, respectively.

The restoring torque $\mathbf{Y}_i$ describes the resistance of the elastic fibers to bending and twisting. The bending and twisting components of this torque are assumed to be linear in the difference between the bending and twisting angles (θ_i and ϕ_i respectively) and their equilibrium values (θ_i^{eq} and ϕ_i^{eq}),

$$|\mathbf{Y}_i| = \kappa_b(\theta_i - \theta_i^{\mathrm{eq}}) + \kappa_t(\phi_i - \phi_i^{\mathrm{eq}}), \tag{3}$$

where κ_b and κ_t are the bending and twisting constants of the fiber. The bending constant is related to the stiffness of the fiber material by $\kappa_b = E_Y I / 2\ell$, where E_Y is the Young's modulus, and $I \equiv \pi b^4/4$ is the area moment. The twisting constant is set to $\kappa_t = 0.67\kappa_b$ in this study, equal to that of a linearly elastic circular cylinder with a Poisson's ratio of 0.5. The fiber flexibility is characterized by a single parameter which we call the effective stiffness, $S^{\mathrm{eff}} \equiv E_Y I / \eta_0 \dot{\gamma} L^4$, where η_0 is the suspending fluid viscosity, $\dot{\gamma}$ is the shear rate, and L is the total fiber length.

Fibers of circular cross-section are assumed to have no preferential bending direction (isotropic bending). However, many fibers, such as refined wood fibers, have a ribbon-like appearance and tend to bend easier in one direction. This may be modelled by defining two orthogonal bending directions with $(\kappa_b)_{\mathrm{hard}} = E_Y I_{\mathrm{hard}} / 2\ell$ and $(\kappa_b)_{\mathrm{easy}} = E_Y I_{\mathrm{easy}} / 2\ell < (\kappa_b)_{\mathrm{hard}}$, as illustrated in Fig. 2. For such anisotropic bending situations, the twisting constant remains fixed at $\kappa_t = 0.67(\kappa_b)_{\mathrm{easy}}$. When $E_Y I_{\mathrm{hard}} \to \infty$, the joint may be modelled as a hinge, resulting in an additional constraint that restricts bending at a joint to that about a preferred axis (e.g., the $\hat{y}$ axis in Fig. 2),

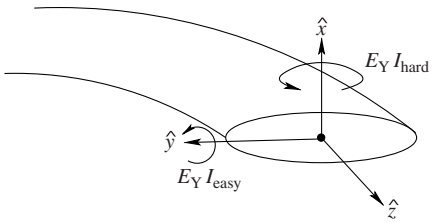

Fig. 2. Schematic illustration of an anisotropic fiber with a preferred bending axis $\hat{y}$. In simulations with anisotropic fibers reported here, the fiber cross-section remains circular.

$$\hat{\mathbf{y}}_i \cdot \mathbf{p}_{i+1} = \cos\theta', \tag{4}$$

where $\hat{\mathbf{y}}_i$ is the preferred bending axis, defined with respect to segment i, and θ' is a constant ($\theta' = \pi/2$ for all simulations with anisotropic bending reported here).

The fiber segments remain connected by applying a constraint for each joint,

$$\mathbf{r}_i + \ell\mathbf{p}_i = \mathbf{r}_{i+1} - \ell\mathbf{p}_{i+1}, \tag{5}$$

where $\mathbf{r}_i$ is the position of the center of segment i. These constraint equations allow for the solution of the constraint forces $\mathbf{X}_i$ at each joint. Since the segments are rigid and remain connected, the fibers are inextensible (but still flexible).

Fibers experience mechanical contacts with other fibers in the suspension. Two fiber segments i and k are considered to be in contact if the separation between their surfaces, h_{ik}, is less than $0.33b$. The force that results from each contact is decomposed into two components—a force in the normal direction of the contact ($\mathbf{F}_{ik}^{\mathrm{N}}$) and a frictional force ($\mathbf{F}_{ik}^{\mathrm{fric}}$) in the plane of the contact. The purely repulsive normal force exerted on segment i by segment k is modelled as $\mathbf{F}_{ik}^{\mathrm{N}} = -F\exp[-ah_{ik}]\mathbf{n}_{ik}$, where $\mathbf{n}_{ik}$ is the unit normal vector directed from segment i to k, $F = 900\pi\eta_0\ell b\dot{\gamma}$ is the force magnitude, and $a = 20/b$. The friction force is determined by the constraint of no relative motion in the plane of contact,

$$\begin{pmatrix} \Delta\mathbf{u}_{ik} \cdot \mathbf{e}_1^{\mathrm{loc}} \\ \Delta\mathbf{u}_{ik} \cdot \mathbf{e}_2^{\mathrm{loc}} \\ \mathbf{F}_{ik}^{\mathrm{fric}} \cdot \mathbf{n}_{ik} \end{pmatrix} = \mathbf{0}, \tag{6}$$

where $\Delta\mathbf{u}_{ik}$ is the relative velocity between segments i and k at the point of contact, and the plane of contact is defined by the vectors $\mathbf{e}_1^{\mathrm{loc}}$ and $\mathbf{e}_2^{\mathrm{loc}}$. The calculated friction force is then subjected to a Coulombic friction law of the form

$$\begin{aligned} &|\mathbf{F}_{ik}^{\mathrm{fric}}| \leqslant \mu^{\mathrm{stat}}|\mathbf{F}_{ik}^{\mathrm{N}}| \Rightarrow \text{contact remains intact} \\ &\quad > \mu^{\mathrm{stat}}|\mathbf{F}_{ik}^{\mathrm{N}}| \Rightarrow \mathbf{F}_{ik}^{\mathrm{fric}} = \mu^{\mathrm{kin}}|\mathbf{F}_{ik}^{\mathrm{N}}|\frac{\Delta\mathbf{u}_{ik}}{|\Delta\mathbf{u}_{ik}|}, \end{aligned} \tag{7}$$

where μ^{stat} and μ^{kin} are the static and kinetic coefficients of friction.

The equations of motion and the constraint equations for all of the fiber segments in the suspension can be expressed as a system of differential algebraic equations (DAEs) for the unknown coordinates and constraint forces,

$$\begin{aligned} &\dot{\mathbf{q}} - \mathbf{F}(\mathbf{q}, \lambda) = \mathbf{0}, \\ &\Psi(\mathbf{q}) = \mathbf{0}, \\ &\Xi(\mathbf{q}, \dot{\mathbf{q}}, \lambda) = \mathbf{0}, \end{aligned} \tag{8}$$

where $\mathbf{q}$ is a vector containing the generalized coordinates of each fiber segment (positions and orientations), and λ is a vector containing all the constraint forces ($\mathbf{X}$ and $\mathbf{F}^{\text{fric}}$) in the suspension. If the segment orientations are represented by Euler parameters (Wittenburg, 1977), there are $7N_{\text{fib}}N_{\text{seg}}$ equations of motion to be solved. The inextensibility constraint (Eq. (5)) represented by the vector Ψ, is made up of $3N_{\text{fib}}(N_{\text{seg}} - 1)$ constraint equations that depend on only the positions and orientations. The $3N_{\text{C}}$ friction constraint equations (Eq. (6)) are contained in Ξ, where N_{C} is the total number of contacts in the system.

Simulations are performed by randomly placing fibers at their equilibrium shape into a cubic simulation cell of size $(\zeta L)^3$, where ζ is the cell size scaling factor ($1.5 \leqslant \zeta \leqslant 4$). A linear shear field is imposed and periodic boundary conditions are applied with the Lees–Edwards modification for shearing systems (Allen and Tilldesley, 1991), to simulate an infinite suspension. The fiber motions are obtained by the numerical solution of the system of DAEs in Eq. (8). An approximate solution method was developed to solve this system, the details of which are described elsewhere (Schmid et al., 2000; Switzer, 2002).

3. Results and discussion

3.1. Illustration of flocculation via friction

Suspensions of flexible fibers in simple shear flow were simulated for a variety of values of the parameters introduced in the previous section. Consider first the behavior of fibers that bend isotropically with $N_{\text{seg}} = 5$, aspect ratio $r_{\text{p}} = 75$, concentration $nL^3 = 20$, and that interact only via short-range repulsive forces and static friction ($\mu^{\text{kin}} = 0$ throughout this article, unless specifically stated otherwise). This model is similar to that studied by Schmid et al. (2000). As reported therein, this system can flocculate for certain ranges of values of the remaining parameters (fiber shape, stiffness, and coefficient of static friction), even though attractive forces between fibers are absent, as illustrated in Fig. 3.

In Fig. 3(a), the coefficient of friction is large ($\mu^{\text{stat}} = 20$), the fibers are relatively stiff ($S^{\text{eff}} = 0.05$), and the equilibrium shape is not straight ($\theta^{\text{eq}} = 0.8$, $\phi^{\text{eq}} = 0.7$). The resulting suspension structure is heterogeneous, with two fiber flocs apparent in the simulation box. For each of Fig. 3(b)–(d), one of the above features is removed, and as a result, the suspension structure remains homogeneous in simple shear flow. In Fig. 3(b), the equilibrium shape is straight ($\theta^{\text{eq}} = \phi^{\text{eq}} = 0$); in Fig. 3(c), friction is absent ($\mu^{\text{stat}} = 0$); and in Fig. 3(d), the fibers are more flexible ($S^{\text{eff}} = 0.0005$). Thus the parameter values employed in Fig. 3(a) are sufficient to achieve flocculation in sheared suspensions. The effects of these parameters, as well as others, on the suspension structure are probed in more detail below. We note that the conditions necessary to observe flocculation are insensitive to the box size and the initial configuration of fibers (Schmid et al., 2000; Schmid and Klingenberg, 2000b).

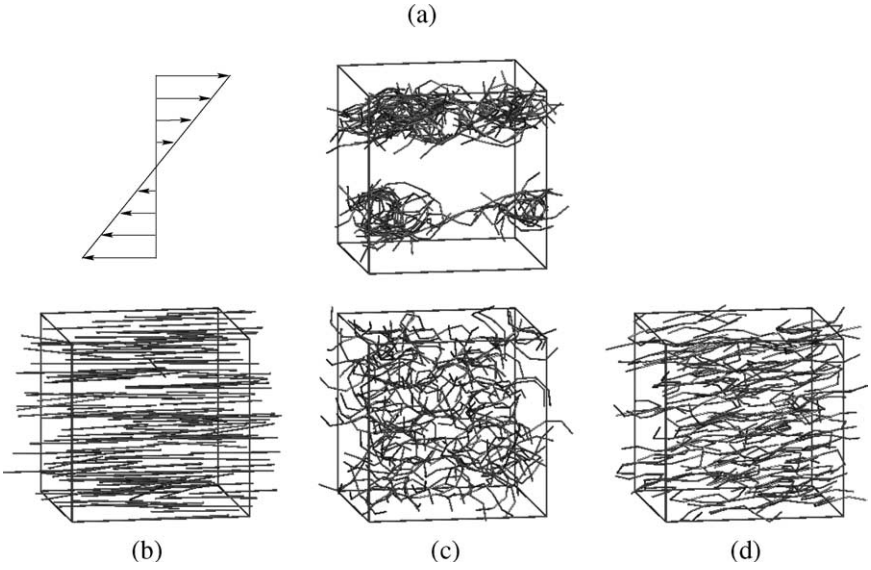

Fig. 3. Simulation snapshots after shearing to a strain of $\gamma = 1500$, with parameters $nL^3 = 20$, $r_p = 75$, $N_{seg} = 5$, and (a) $\mu^{stat} = 20$, $S^{eff} = 0.05$, $\theta^{eq} = 0.8$, $\phi^{eq} = 0.7$ (flocculated suspension); (b) same as (a) except $\theta^{eq} = \phi^{eq} = 0$; (c) same as (a) except $\mu^{stat} = 0$; and (d) same as (a) except $S^{eff} = 0.0005$.

The suspension structure can be characterized quantitatively by the pair distribution function of the fiber centers-of-mass, $g(r)$, and the average number of contacts per fiber, $\langle n_c \rangle$. The pair distribution functions are plotted as a function of separation in Fig. 4(a) for the systems depicted in Fig. 3. Here, the pair distribution functions are averaged over all angular positions. For the homogeneous suspensions, there is an equal probability of finding fiber pair centers-of-mass with any separation. The flocculated suspension, however, has a high probability of finding fiber centers at small separations.

The pair distribution function can be used to identify systems that flocculate. For suspensions that flocculate by varying the value of one parameter (e.g., μ^{stat}, nL^3, or the fiber shape), the transition from a homogeneous to a heterogeneous suspension is dramatic and occurs over a fairly narrow range of parameter values (Schmid et al., 2000). For homogeneous suspensions, $g(r)$ resembles curves (b), (c) or (d) in Fig. 4(a). As a parameter is varied such that snapshots of the suspension become visibly heterogeneous, $g(r)$ always attains a shape similar to that depicted by curve (a) of Fig. 4(a), with $g(r = 0.01L) \geqslant 3$. We thus find it convenient to define a system as flocculated if $g(r = 0.01L) \geqslant 3$. This definition allows us to easily monitor the degree of heterogeneity quantitatively during simulations. Other measures of the microstructure could certainly be employed (e.g., the integral of $g(r)$, or the structure factor), but we have found that the definition $g(r = 0.01L) \geqslant 3$ has not failed to distinguish a heterogenous structure from a homogeneous one (as determined from visual inspection of snapshots).

The average number of contacts per fiber is plotted as a function of shear strain γ in Fig. 4(b) for each of the systems in Fig. 3. For the non-flocculated systems, $\langle n_c \rangle$ rapidly achieves a constant, steady-state value. For the flocculated system, $\langle n_c \rangle$ increases to a constant steady-state value greater than those for the non-flocculated system, over a strain of several hundred. Monitoring

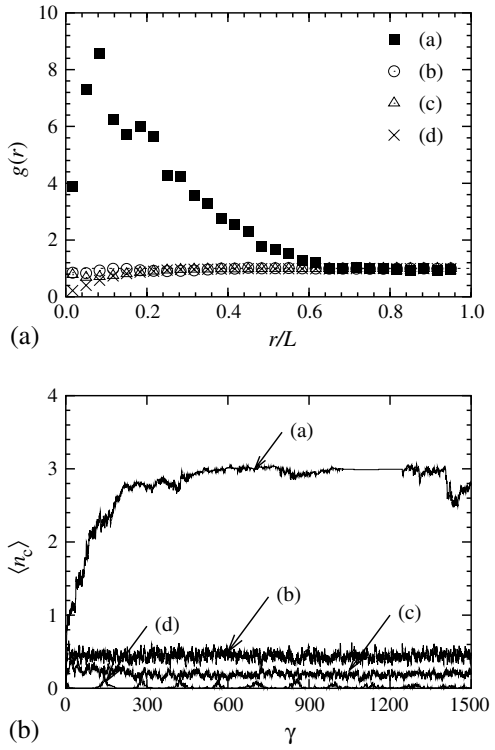

Fig. 4. (a) Pair distribution function, and (b) average number of contacts per fiber versus strain for the runs depicted in Fig. 3.

$\langle n_c(\gamma)\rangle$ during a simulation run is an effective way of determining when steady state is achieved. The steady-state value of $\langle n_c\rangle$ also describes the extent to which a fiber network is formed. Meyer and Wahren (1964) defined a fiber network as a system of fibers in which each fiber is held in position by contact with at least three other fibers. This is consistent with the flocculated system illustrated in Fig. 3(a), where $\langle n_c\rangle \approx 3$ at steady state.

3.2. Effects of friction and fiber stiffness

Fibers in contact interact via friction forces characterized by a static coefficient of friction, μ^{stat}. For $\mu^{\text{stat}} = 0$, the suspension structure remains homogeneous regardless of the other parameter values. As illustrated in Fig. 3, for certain ranges of parameter values, suspensions will tend to flocculate for sufficiently large values of μ^{stat}. For such systems, as μ^{stat} is increased from zero above $\mu^{\text{stat}}_{\text{min}}$, which depends on the other parameter values, suspensions begin to show increased heterogeneity. For the parameter values $(N_{\text{seg}}, r_p, nL^3, S^{\text{eff}}, \theta^{\text{eq}}, \phi^{\text{eq}}) = (5, 75, 20, 0.05, 0.8, 0.7)$, $\mu^{\text{stat}}_{\text{min}} \approx 5$. As μ^{stat} is increased further, the degree of heterogeneity increases; however, for $\mu^{\text{stat}} \geqslant \mu^{\text{stat}}_{\text{max}}$, the structure as characterized by $g(r = 0.01L)$ or $\langle n_c(\gamma \to \infty)\rangle$ no longer changes appreciably. The value of $\mu^{\text{stat}}_{\text{max}}$ is also a function of the other parameter values; for the values listed

above, $\mu^{\text{stat}}_{\text{max}} \approx 10$. For most simulated flexible fiber suspensions that we have observed to flocculate, $10 < \mu^{\text{stat}}_{\text{max}} < 100$ (Switzer, 2002).

Similar behavior is observed as the fiber flexibility is varied. All suspensions will remain homogenous for sufficiently small effective stiffness ($S^{\text{eff}} \equiv E_{\text{Y}} I/\eta_0 \dot{\gamma} L^4 \ll 1$). As illustrated in Fig. 3, some suspensions will flocculate when the effective stiffness is increased above a certain value (which depends on the other parameter values).

The requirement of both a sufficiently large effective fiber stiffness and a sufficiently large coefficient of friction in order to produce heterogeneous structures is consistent with the elastic-interlocking mechanism of flocculation proposed by Kerekes et al. (1985) (also called Type-C cohesion). They proposed that the cohesive forces that hold fibers within flocs are caused by interfiber friction. The strength of the friction force is proportional to the normal force between contacting fibers, and this normal force is a function of the fiber stiffness. Soszynski and Kerekes confirmed this mechanism experimentally; nylon fiber flocs readily dispersed when the fiber stiffness was reduced by heating above the glass transition temperature of nylon. Schmid et al. (2000) reported similar behavior using a model and simulation method similar to those employed here. Flocs formed in simple shear become trapped in elastically strained configurations upon cessation of shear. When the flocs are extracted from the simulation box and placed in an unbounded shear flow, the floc slowly disperses. If the effective fiber stiffness or the coefficient of friction is reduced, the fibers disperse much more rapidly (Schmid et al., 2000; Switzer, 2002).

Although the simulation results presented thus far appear to agree with experimental observations, unreasonably large values of μ^{stat} are necessary to see flocculation for the conditions described above ($\mu^{\text{stat}} > 1$). The value of μ^{stat} measured experimentally for contacting cellulose surfaces and cellulose fibers is approximately 0.5 (Amelina et al., 1998; Shchukin et al., 1998; Zauscher and Klingenberg, 2001). However, we also find that the effective stiffness values employed thus far are small compared to those typically achieved in experiments. Choosing dimensional parameter values typical for wood fibers sheared in water ($E_{\text{Y}} I \approx 10^{-12}$ N m^2 (Tam Doo and Kerekes, 1981), $L \approx 2.3$ mm, $d \approx 30$ μm, $\eta_0 = 0.001$ Pa s, $\dot{\gamma} \simeq 10$), the dimensionless stiffness is $S^{\text{eff}} \approx 4$. This is much larger than the values used in the simulations with equivalent aspect ratios ($r_{\text{p}} = 75$). Simulating suspensions of fibers this stiff requires a very small time step ($\dot{\gamma} \Delta t < 10^{-8}$) and thus significantly more computational power than is currently available to simulate to shear strains $\gamma > 1000$.

To probe the behavior of flocculating suspensions composed of much stiffer fibers, we investigated the behavior of a test floc made up of five inherently straight fibers interwoven into a "star" configuration (illustrated in the inset of Fig. 5; $N_{\text{seg}} = 7$, $r_{\text{p}} = 56$, $\theta^{\text{eq}} = 0$, $\phi^{\text{eq}} = 0$) similar to the test structure proposed by Farnood et al. (1994). The test floc was placed in a simple shear field and sheared to a strain $\gamma = 100$ (in the plane of shear). For a fixed value of S^{eff}, the test floc would remain intact if μ^{stat} were large enough, and the test floc would disperse if μ^{stat} were too small. The minimum value of μ^{stat} necessary keep the floc intact was defined as a "critical" friction coefficient, $\mu^{\text{stat}}_{\text{crit}}$, which is a function S^{eff}. The critical friction coefficient is plotted as a function of S^{eff} for the star in Fig. 5. As the stiffness increases, the coefficient of friction necessary to hold the floc together decreases. These results suggest that for large values of S^{eff}, comparable to those typically encountered experimentally ($S^{\text{eff}} > 1$), the coefficient of friction necessary to see flocculation in simulations of sheared suspensions may indeed approach the coefficient of friction values measured experimentally.

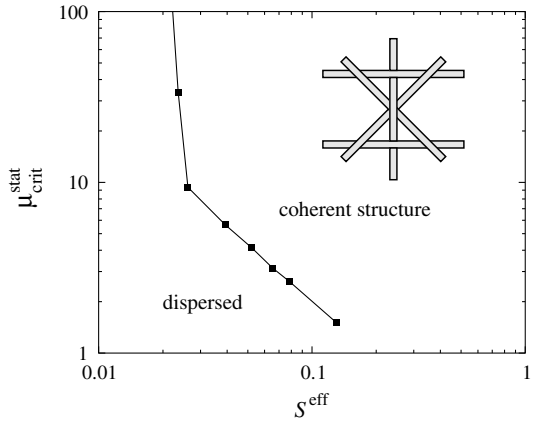

Fig. 5. Critical coefficient of friction as a function of the effective stiffness for the star test floc in simple shear flow, $(N_{seg}, r_p, \theta^{eq}, \phi^{eq}) = (7, 56, 0, 0)$.

Varying the dimensionless stiffness S^{eff} can be achieved by varying the intrinsic fiber stiffness ($E_Y I$), the fiber length (L), the suspending fluid viscosity (η_0), or the shear rate ($\dot{\gamma}$). Soszynski and Kerekes (1988a,b) showed the importance of the effective fiber stiffness in producing flocs in a recirculating flow of nylon fiber suspensions. As η_0 was increased (effective stiffness decreased) the concentration at which flocs first formed (threshold concentration, $(nL^3)_{thr}$) increased. Above a certain value of η_0, flocs would no longer form. This phenomenon was investigated with the simulation method presented here, by shearing suspensions with a fixed effective stiffness to $\gamma = 1500$ and varying concentrations in order to determine the threshold concentration. The results are shown in Fig. 6 where $(nL^3)_{thr}$ is plotted as a function of $1/S^{eff} \propto \eta_0$ for the parameter values $(N_{seg}, r_p, \theta^{eq}, \phi^{eq}, \mu^{stat}) = (5, 75, 0.6, 0, 20)$. The threshold concentration increases as $1/S^{eff}$ increases, with no flocs observed for $1/S^{eff} \gtrsim 500$, qualitatively consistent with the experimental observations reported by Soszynski and Kerekes. Soszynski and Kerekes (1988a) explain the dependence of flocculation tendency on η_0 in terms of a competition between the different forces

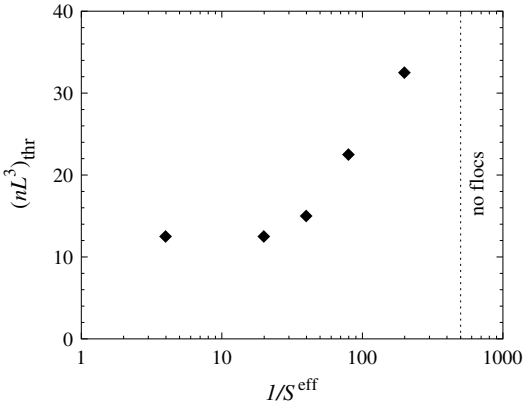

Fig. 6. Threshold concentration to produce flocs as a function of the inverse of the effective stiffness, $1/S^{eff} \propto \eta_0$; $(N_{seg}, r_p, \theta^{eq}, \phi^{eq}, \mu^{stat}) = (5, 75, 0.6, 0, 20)$.

that determine fiber motion. In low η_0 suspending fluids, fiber motion is dominated by fiber interactions (as well as acceleration and deceleration in unsteady flows), and the fibers do not closely follow the suspending fluid motion. In sufficiently concentrated suspensions, this non-affine motion can result in local "crowding," which leads to entanglement and floc formation. The fiber motion in large η_0 fluids is dominated by hydrodynamic forces, resulting in affine motion and perhaps a higher degree of fiber alignment (in shear flows). Crowding is thus inhibited, resulting in no floc formation. This explanation is consistent with the model and simulation results presented here. The relevant dimensionless quantity, the effective stiffness $S^{\text{eff}} = E_{\text{Y}} I/\eta_0 \dot{\gamma} L^4$, characterizes the relative importance of viscous and elastic forces, the latter of which is intimately related to fiber interactions. Furthermore, as illustrated in Fig. 3(a) and (b), decreasing S^{eff} sufficiently (i.e., increasing η_0) clearly results in more aligned structures in addition to a more homogeneous system.

Kerekes (1995) postulated that fluid inertia plays an important role in the formation of flocs in fiber suspensions. Since our model neglects both fluid and fiber inertia, we cannot comment on the role of inertia in flocculation. We can only state that this model predicts that flocs can be produced in shear flow at small Reynolds numbers under appropriate conditions (i.e., inertia is not necessary).

3.3. Effects of fiber shape

The equilibrium shape of a fiber significantly impacts the suspension microstructure. The dependence of fiber equilibrium shape on flocculation behavior has been investigated by performing simulations with suspensions of U-shaped fibers. The shape may be characterized by the common equilibrium angle θ^{eq} ($\phi^{\text{eq}} = 0$) at each joint, or equivalently by the fiber radius of curvature, defined here for linked rigid bodies as

$$R_{\text{U}} = \frac{1}{2}\left(\frac{\ell}{\sin(\theta^{\text{eq}}/2)} + \frac{\ell}{\tan(\theta^{\text{eq}}/2)}\right), \tag{9}$$

where ℓ is the segment half-length. The first term in parentheses is the radius of a circle passing through the ball and socket joints, and the second term is the radius of a circle tangent to the centers of the fiber segments. The radius R_{U} is the average of these two radii.

Suspensions with specific radii of curvature and various concentrations were simulated in simple shear flow to $\gamma = 1500$, with all other parameters fixed ($(N_{\text{seg}}, r_{\text{p}}, S^{\text{eff}}, \mu^{\text{stat}}) = (5, 75, 0.05, 20)$). The results are summarized in Fig. 7(a) where the homogeneity of the suspensions is mapped as a function of curvature and concentration. Suspensions that remained homogeneous are represented by open circles, while suspensions that flocculated are represented by filled circles. Suspensions flocculate at lower concentrations as the dimensionless fiber curvature (b/R_{U}) is increased. As the fibers become nearly straight ($b/R_{\text{U}} \to 0$), the suspensions only flocculate at high concentrations, and perfectly straight fibers have never been observed to produce heterogeneous structures in the simulations. However, it is possible that flocs formed at sufficiently large concentration may exceed the simulation box size, or that there is a transition to the formation of space-filling, elastically interlocked networks (Schmid et al., 2000).

The variation in suspension structure with fiber shape can also be characterized by the average number of contacts per fiber at steady state $\langle n_{\text{c}} \rangle_{\text{ss}}$, as illustrated in Fig. 7(b). Here, $\langle n_{\text{c}} \rangle_{\text{ss}}$ is plotted as a function of b/R_{U} for $N_{\text{seg}} = 3$ and 5, with the remaining parameter values

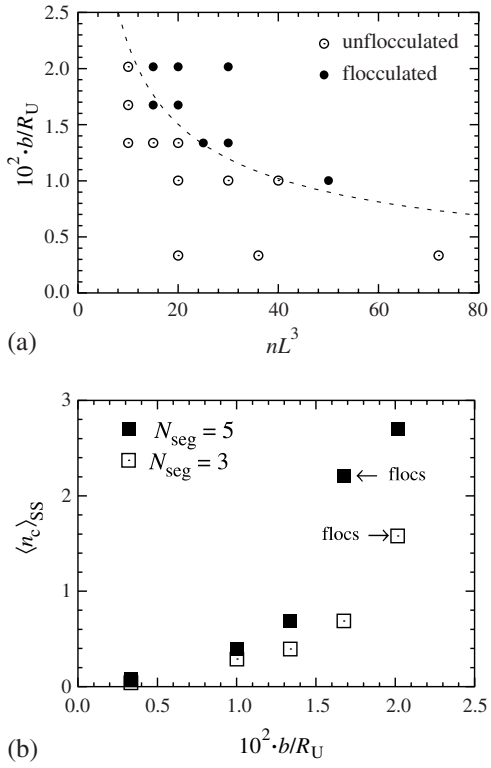

Fig. 7. (a) Suspension homogeneity (at $\gamma = 1500$) mapped as a function of curvature (b/R_U) and concentration ($(N_{seg}, r_p, S^{eff}, \mu^{stat}) = (5, 75, 0.05, 20)$); (b) average number of contacts per fiber at steady state ($\langle n_c \rangle_{ss}$) as a function of b/R_U for suspensions at $nL^3 = 20$ after shearing for $\gamma = 1500$ ($(N_{seg}, r_p, S^{eff}, \mu^{stat}) = (5, 75, 0.05, 20)$).

$(nL^3, S^{eff}, r_p, \mu^{stat}) = (20, 0.05, 75, 20)$. As b/R_U increases (the fibers become more curved), $\langle n_c \rangle_{ss}$ increases. This is likely caused by the decreased rotation period of higher curvature fibers resulting in more interfiber collisions. The values of $\langle n_c \rangle_{ss}$ increase slowly with increasing b/R_U at first. When the curvature becomes large enough to cause flocculation, $\langle n_c \rangle_{ss}$ increases rapidly.

The fiber shape also depends on the number of segments, and thus so do the details of the suspension structure, as illustrated in Fig. 7(b). Flocculation for suspensions of three-segment fibers is shifted to slightly larger curvatures compared to suspensions with five-segment fibers. Suspensions of fibers with $N_{seg} \geqslant 5$ show approximately the same behavior at an aspect ratio of $r_p = 75$, under these conditions. One would expect the influence of the number of segments on the suspension structure to be a function of the fiber aspect ratio and flexibility.

3.4. Effects of kinetic friction

All of the results presented thus far employ only the static friction constraint ($\mu^{kin} = 0$ in Eq. (7)); if the force required to keep contacting segments i and k from sliding exceeds $\mu^{stat}|\mathbf{F}^N_{ik}|$, the segments are allowed to slide unimpeded (except for hydrodynamic drag). To investigate the influence of kinetic friction on suspension structure, shear flow was simulated for the parameter

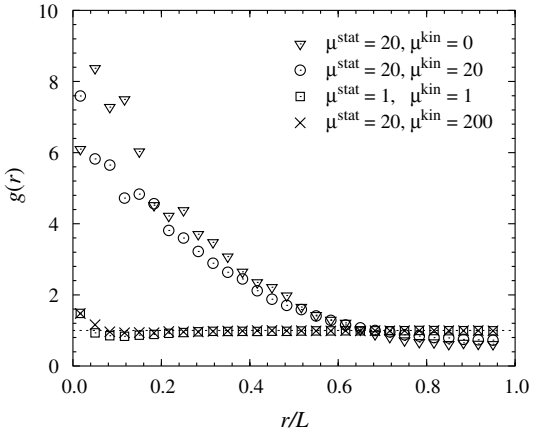

Fig. 8. Pair distribution function for the fiber centers-of-mass of suspensions in simple shear flow at steady state $\gamma > 1000$, for various values of the coefficients of static and kinetic friction $(N_{\text{seg}}, r_{\text{p}}, nL^3, S^{\text{eff}}, \theta^{\text{eq}}, \phi^{\text{eq}}) = (5, 75, 20, 0.05, 0.6, 0)$.

values $(N_{\text{seg}}, r_{\text{p}}, nL^3, S^{\text{eff}}, \theta^{\text{eq}}, \phi^{\text{eq}}) = (5, 75, 20, 0.05, 0.6, 0)$, and various values of μ^{stat} and μ^{kin}. The steady-state pair distribution functions for some of these simulations are plotted in Fig. 8, and the results are summarized below.

In the absence of kinetic friction ($\mu^{\text{kin}} = 0$), flocculation only occurs for $\mu^{\text{stat}} \geqslant \mu^{\text{stat}}_{\text{min}} \approx 10$. Such behavior is illustrated in Fig. 8, where the pair distribution function for a simulation with $\mu^{\text{stat}} = 20$ and $\mu^{\text{kin}} = 0$ exhibits a flocculated structure ($g(r = 0.01L) \approx 9$). Adding sliding friction does not substantially influence the structure, as illustrated by the similar pair distribution function for $\mu^{\text{stat}} = 20$ and $\mu^{\text{kin}} = 20$.

Consider next the "incipient" situation where $\mu^{\text{stat}} = 1$, which is less than that required to observe flocculation ($\mu^{\text{kin}} = 0$). The addition of kinetic friction with $\mu^{\text{kin}} = \mu^{\text{stat}} = 1$ is not sufficient to cause the suspension to flocculate. This is illustrated in Fig. 8 where the pair distribution function for this case reflects a homogeneous structure. Similar behavior is observed for all simulations with $\mu^{\text{kin}} \leqslant \mu^{\text{stat}} < \mu^{\text{stat}}_{\text{min}}$. We thus conclude that kinetic friction does not significantly influence flocculation behavior. In other words, kinetic friction cannot significantly reduce the coefficient of static friction necessary to induce flocculation.

Not only is kinetic friction unable to induce flocculation in nearly flocculated systems, but the addition of kinetic friction can actually inhibit flocculation when $\mu^{\text{kin}} \gg \mu^{\text{stat}} > \mu^{\text{stat}}_{\text{min}}$. This is illustrated in Fig. 8 in which the pair distribution function for $\mu^{\text{stat}} = 20$ and $\mu^{\text{kin}} = 200$ characterizes a structure less heterogenous than that obtained for $\mu^{\text{stat}} = 20$ and $\mu^{\text{kin}} = 0$.

While kinetic friction can affect the suspension structure, it apparently does not significantly influence flocculation behavior. Thus in the remainder of this article, only results from simulations with $\mu^{\text{kin}} = 0$ are reported.

3.5. Effect of weak attractive forces

All of the simulations discussed thus far have been performed in the absence of attractive forces between fibers. However, experiments have shown that weak attractive forces can exist between

fibers in suspension. Shchukin et al. (1998) reported attractive force magnitudes of $|\mathbf{F}^{\text{att}}| \approx 0.04$ μN for cellulose fibers in water, and Chaouche and Koch (2001) reported attractive force magnitudes in the range $|\mathbf{F}^{\text{att}}| \approx 0.01$–6 μN for nylon fibers in various fluids. While attractive forces may themselves cause aggregation, they may also serve to lower the coefficient of friction necessary to see friction-induced flocculation. To model attractive forces in the simulations, we added a weak attractive term to the normal force between fibers $\mathbf{F}_{ik}^{\text{N}} = -6\pi\eta_0\ell b\dot{\gamma}[F\exp(-ah) - A_{\text{N}}\exp(-a_{\text{A}}h^2)]\mathbf{n}_{ik}$, where A_{N} is the dimensionless magnitude of the attractive force and a_{A} is related to the decay length of the attractive force. The parameter values were selected so that the maximum attractive force is $|\mathbf{F}_{\max}^{\text{N}}| \approx 0.02$ μN (for $F = 150$, $a = 20$, $A_{\text{N}} = 9$, and $a_{\text{A}} = 35$, and the suspension parameters $\eta_0 = 1$ Pa s, $L = 2\ell N_{\text{seg}} = 2.5$ mm, $b = 16$ μm, and $\dot{\gamma} = 10$ s^{-1}). The structures of suspensions in simple shear flow with purely repulsive interactions ($A_{\text{N}} = 0$) and with weak attractive forces ($A_{\text{N}} = 9$) are compared in Fig. 9 where the steady-state pair distribution functions are presented for various values of μ^{stat} and the remaining parameters values fixed at $(N_{\text{seg}}, r_{\text{p}}, nL^3, S^{\text{eff}}, \theta^{\text{eq}}, \phi^{\text{eq}}, \mu^{\text{kin}}) = (5, 75, 20, 0.05, 0.8, 0.7, 0)$. With $\mu^{\text{stat}} = 5$, suspensions with and without attractive forces flocculate. The fibers with weak attractive forces have a slightly higher probability of having small separations between the fiber centers-of-mass than fibers with purely repulsive interactions ($g(r = 0.01L) \approx 8$ and $g(r = 0.01L) \approx 6$ for $A_{\text{N}} = 9$ and $A_{\text{N}} = 0$, respectively). However, for $\mu^{\text{stat}} = 1 < \mu_{\min}^{\text{stat}} \approx 5$, the pair distribution functions reflect a homogeneous structure for both $A_{\text{N}} = 0$ and $A_{\text{N}} = 9$. Thus weak attractive forces do not significantly alter the minimum coefficient of friction necessary to induce flocculation.

Schmid (1999) demonstrated the effect of using larger attractive forces between fibers ($|\mathbf{F}_{\max}^{\text{N}}| \approx 10$ μN) in the absence of friction ($\mu^{\text{stat}} = \mu^{\text{kin}} = 0$). Although larger attractive forces did lead to flocculation in the absence of friction, the behavior of the systems was markedly different than that exhibited by systems that flocculate by friction. The fibers did not elastically interlock, as observed experimentally (Soszynski and Kerekes, 1988a,b). In particular, increasing the effective stiffness lead to a less coherent structure. Thus attractive forces alone cannot explain the

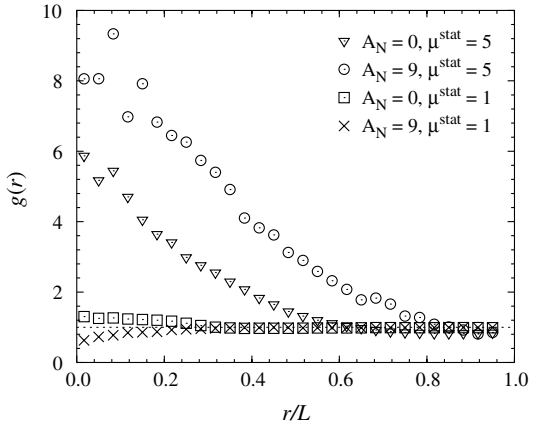

Fig. 9. Pair distribution function for the fiber centers-of-mass of suspensions in simple shear flow at steady state $\gamma > 1000$, with and without attractive potentials $(N_{\text{seg}}, r_{\text{p}}, nL^3, S^{\text{eff}}, \theta^{\text{eq}}, \phi^{\text{eq}}) = (5, 75, 20, 0.05, 0.8, 0.7)$.

observation reported by Soszynski and Kerekes (1988a) that reducing elastic stresses leads to less coherent structures.

Chaouche and Koch (2001) observed flocculation in suspensions of nearly straight nylon fibers in viscous fluids with smaller aspect ratios ($r_p \approx 36$) sheared at very low shear rates ($\dot{\gamma} \ll 1$). They hypothesized that flocculation was due to attractive forces between fibers because the fibers were sufficiently stiff to be considered rigid rods, suggesting that they could not deform and elastically interlock ($S^{\text{eff}} \gg 1$). Simulations of perfectly rigid, straight fibers both with ($A_N = 9$) and without weak attractive forces at conditions similar to those employed by Chaouche and Koch ($r_p = 35$ and $nL^3 \approx 17$–52) were performed, along with similar simulations of suspensions of straight and curved flexible fibers of the same aspect ratio, with and without attractive forces ($(N_{\text{seg}}, r_p, nL^3, S^{\text{eff}}, \theta^{\text{eq}}, \phi^{\text{eq}}, \mu^{\text{stat}}) = (5, 75, 17\text{–}52, 0.7, 0\text{–}0.1, 0, 20)$). In Fig. 10, the pair distribution functions are presented for the various simulations with $nL^3 = 52.4$. In each case (as well as at smaller concentrations), the structures remain homogeneous. Thus the addition of attractive forces does not cause the suspensions to flocculate, in the sense of producing heterogeneous structures. However, the simulations with flexible fibers could not be performed at the large values of the effective stiffness reported by Chaouche and Koch ($S^{\text{eff}} \approx 2000$); it is possible that the simulations could produce flocs at larger values of S^{eff} if such simulations could be performed.

Although the simulations described above did not produce heterogeneous structures, the addition of attractive forces does influence the suspension behavior in other ways. In Fig. 11, the specific viscosity is plotted as a function of concentration for the simulations described above, with and without attractive forces. (The specific viscosity is defined $\eta_{\text{sp}} \equiv (\eta - \eta_0)/\eta_0$, where η is the shear viscosity of the suspension. The methods used to calculate the rheological properties of flexible fiber suspensions are described elsewhere (Switzer and Klingenberg, 2003).) The addition of attractive forces causes a significant increase in the specific viscosity, consistent with the observations of Chaouche and Koch. The influence of attractive forces on the specific viscosity is more significant for flexible fibers than for straight, rigid fibers. The specific viscosity of the curved fiber suspensions is not altered significantly, but remains larger than the viscosity of straight fiber

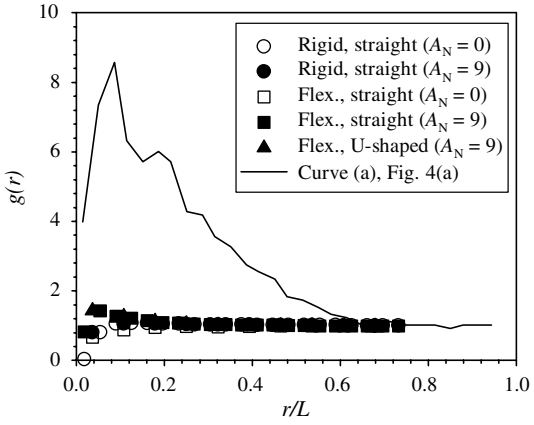

Fig. 10. Pair distribution functions for simulations of various fiber suspensions with $r_p = 35$, $\mu^{\text{stat}} = 20$, and $nL^3 = 52.4$. Rigid fibers: $N_{\text{seg}} = 1$; flexible, straight fibers: $N_{\text{seg}} = 5$, $S^{\text{eff}} = 0.7$; U-shaped fibers: $N_{\text{seg}} = 5$, $S^{\text{eff}} = 0.7$, $\theta^{\text{eq}} = 0.1$. Also shown is the pair distribution function for a flocculated suspension (curve (a) in Fig. 4(a)).

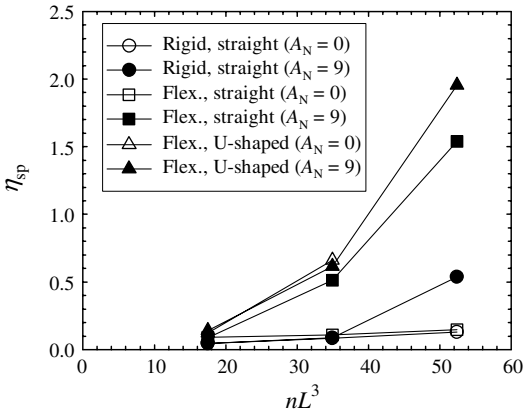

Fig. 11. Specific viscosity as a function of fiber concentration for various suspensions with $r_p = 35$ and $\mu^{stat} = 20$, with and without attractive forces. Rigid fibers: $N_{seg} = 1$; flexible, straight fibers: $N_{seg} = 5$, $S^{eff} = 0.7$; U-shaped fibers: $N_{seg} = 5$, $S^{eff} = 0.7$, $\theta^{eq} = 0.1$.

suspensions. The increase in viscosity of the straight fiber suspensions appears to be caused by a change in the suspension microstructure—not the formation of heterogeneous structures, but rather a change in the orientation distribution. In Fig. 12, the average of the *xz* component of the orientation tensor $\langle \mathbf{pp} \rangle$ ($\mathbf{p}$ is the orientation vector of the major axis of a segment) is plotted as a function of concentration for the simulations described above. The addition of attractive forces causes segments of straight fibers to spend more time oriented away from the direction of flow ($p_z \neq 0$), giving rise to an increased specific viscosity. The orientation of the curved fiber suspensions is not altered significantly by attractive forces, and the viscosity remains essentially unchanged. Thus while attractive forces do not cause flocculation in these systems—in the sense of producing heterogeneous structures—they do alter the structure and rheology of the straight fiber suspensions in manner consistent with the observations of Chaouche and Koch.

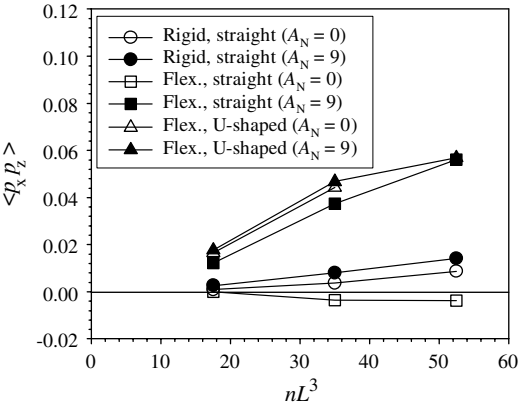

Fig. 12. *xz* component of the orientation tensor $\langle \mathbf{pp} \rangle$ as a function of fiber concentration for various suspensions with $r_p = 35$ and $\mu^{stat} = 20$, with and without attractive forces. Rigid fibers: $N_{seg} = 1$; flexible, straight fibers: $N_{seg} = 5$, $S^{eff} = 0.7$; U-shaped fibers: $N_{seg} = 5$, $S^{eff} = 0.7$, $\theta^{eq} = 0.1$.

3.6. Effect of anisotropic bending

We investigated the effect of changing the bending stiffness in the joints such that the fibers have a preferential bending direction (anisotropic bending). The fiber joints were changed from ball and socket joints to pin joints, which constrain the motion of adjacent fiber segments to a plane. This makes the effective stiffness infinite for a restoring torque parallel to the plane ($(S^{\text{eff}})_{\text{hard}} \to \infty$), while allowing the effective stiffness for bending perpendicular to the plane ($(S^{\text{eff}})_{\text{easy}}$) to remain finite.

The pair distribution functions for the fiber centers-of-mass for suspensions of isotropic fibers ($S^{\text{eff}} = 0.05$) at $\mu^{\text{stat}} = 20$ and for suspensions of anisotropic fibers with pin joints ((A) $(S^{\text{eff}})_{\text{easy}} = 0.05$, $\mu^{\text{stat}} = 20$; (B) $(S^{\text{eff}})_{\text{easy}} = 0.05$, $\mu^{\text{stat}} \to \infty$; and (C) $(S^{\text{eff}})_{\text{easy}} = 0.01$, $\mu^{\text{stat}} = 20$), in which all other variables are held constant ($(N_{\text{seg}}, r_{\text{p}}, nL^3, \theta^{\text{eq}}, \phi^{\text{eq}}, \mu^{\text{kin}}) = (5, 75, 20, 0.6, 0, 0)$), are plotted in Fig. 13. The anisotropically bending fibers (A), result in a relatively homogeneous suspension at steady state, in contrast to the isotropic fibers that flocculate strongly at the same conditions. Increasing the coefficient of friction for the anisotropic fibers to infinity (B) results in a flocculated suspension, although it is less heterogeneous than the equivalent suspension of isotropic fibers with $\mu^{\text{stat}} = 20$. Decreasing the effective stiffness in the bending direction also results in a homogeneous distribution of fibers (C). If the pin joints are replaced by anisotropic ball and socket joints with $(S^{\text{eff}})_{\text{hard}} = 5(S^{\text{eff}})_{\text{easy}} = 0.25$ or $(S^{\text{eff}})_{\text{hard}} = 2(S^{\text{eff}})_{\text{easy}} = 0.1$ with all other conditions the same as those given above, the suspension no longer flocculates.

At present, we are unable to explain the behavior observed for simulations of anisotropically bending fibers. One possible explanation for this change in flocculation behavior may be that the number of configurations the anisotropic fibers can assume is too limited to allow the fibers to entangle and interlock. However, wood fibers have ribbon-like structures which give them preferential bending directions, and wood fibers will flocculate. While the model does take into account preferential bending, the real fiber geometry is not considered. These "flattened" wood fibers can contact one another at much larger areas than our model fibers (circular cross-section), which may

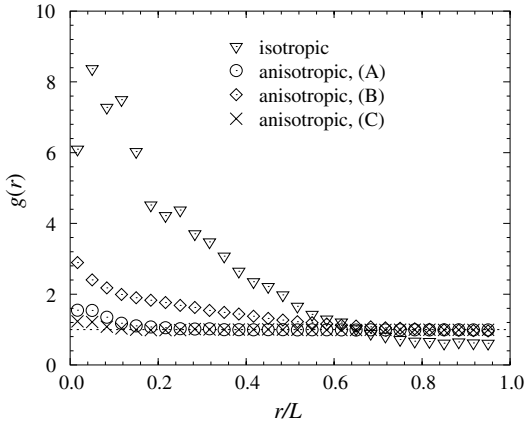

Fig. 13. Pair distribution function for the centers-of-mass of fibers with isotropic ($S^{\text{eff}} = 0.05$, $\mu^{\text{stat}} = 20$) and anisotropic bending ((A) $(S^{\text{eff}})_{\text{easy}} = 0.05$, $\mu^{\text{stat}} = 20$; (B) $(S^{\text{eff}})_{\text{easy}} = 0.05$, $\mu^{\text{stat}} \to \infty$; and (C) $(S^{\text{eff}})_{\text{easy}} = 0.01$, $\mu^{\text{stat}} = 20$) using pin joints after shearing for $\gamma = 1500$ with $(N_{\text{seg}}, r_{\text{p}}, nL^3, \theta^{\text{eq}}, \phi^{\text{eq}}, \mu^{\text{kin}}) = (5, 75, 20, 0.6, 0, 0)$.

result in enhanced frictional interactions or even bonding. Indeed, the model has shown that anisotropic fibers will flocculate by substantially increasing μ^{stat}. Also, real fibers have a distribution of lengths, stiffnesses, cross-sectional areas, and shapes that we have not considered in the results reported here.

4. Conclusions

We have employed a model for flexible fibers and a particle-level simulation technique to investigate the relationships between fiber properties, interactions, and the structure of non-Brownian, flexible fiber suspensions in simple shear flow. The fiber model includes such realistic features as non-straight equilibrium shapes, flexibility, and frictional contacts. Each fiber is composed of a series of linked rigid spherocylinders connected by ball and socket joints.

The main conclusions from this study are as follows:

- The simulations show that suspensions of flexible fibers interacting via frictional contacts can flocculate, even in the absence of attractive interfiber forces. The flocculation process observed is consistent with the elastic-interlocking mechanism proposed by Soszynski and Kerekes (1988a). The tendency toward flocculation depends on several parameters. A suspension of fibers that are too flexible, or whose coefficient of static friction is too small will not flocculate, regardless of the values of the remaining parameters. The minimum coefficient of friction necessary to observe flocculation appears to decrease as the fiber stiffness increases.
- The dependence of the homogeneity of the suspension structure on the dimensionless fiber stiffness (effective stiffness, $S^{\text{eff}} \equiv E_{\text{Y}} I/\eta_0 \dot{\gamma} L^4$) agrees qualitatively with numerous experimental observations.
- Fiber shape also influences the suspension structure, as the concentration at which fibers begin to flocculate decreases with increasing fiber curvature (for U-shaped fibers).
- Other parameters have a weaker influence on the suspension structure. Kinetic (sliding) friction and weak attractive forces have little effect on the structural behavior of fiber suspensions (for the ranges of parameter values investigated). Anisotropic bending tends to shift the onset of flocculation to larger values of the coefficient of static friction.

The most important practical implications of the results are threefold. First, we have provided support to the previous conjecture that flocculation can indeed arise from friction alone, in the absence of attractive forces between fibers. This, and the ability to reproduce other experimental observations (e.g., effects of fiber stiffness) help to establish the validity of fiber-level simulations. Second, this simulation method can be employed to explore effects of properties and conditions that are very difficult to investigate in a systematic way experimentally. For example, it is very challenging to systematically explore the influence of fiber shape on suspension structure experimentally, but this is quite straightforward in simulations. Finally, because experiments can be very time-consuming and costly, simulations can be used to guide experiments, thus significantly reducing their number and the associated cost. This requires, of course, that the ability of simulations to produce qualitatively or quantitatively correct results is established. While achieving

quantitative prediction capabilities with simulations is a reasonable goal, even qualitative prediction capabilities can be extremely useful for reducing experimental efforts (Nilsen et al., 1998).

The main limitation of this approach is the computational demand. The maximum allowable time step (for obtaining stable, accurate solutions to the DAEs) decreases with increasing fiber stiffness, which limits simulations with many fibers to relatively small stiffnesses, well below that expected in many practical situations of interest. Improving the computation speed will not only allow us to investigate more realistic fiber stiffnesses, but also to investigate a greater range of parameter space.

Acknowledgements

This research was supported in part by the USDA NRI Competitive Grants Program (award no. 2001-35103-09933).

References

Allen, M.P., Tilldesley, D.J., 1991. Computer Simulation of Liquids. Oxford Science Publications.

Almin, K.E., Biel, P., Wahren, D., 1967. An experimental investigation of the shear modulus of model fibre networks. Sven. Papperstidn. 67, 772–774.

Amelina, E.A., Shchukin, E.D., Parfenova, A.M., Bessonov, A.I., Videnskii, I.V., 1998. Adhesion of the cellulose fibers in liquid media:1. Measurement of the contact friction force. Colloid J. 60, 537–540.

Beghello, L., 1998. The Tendency of Fibers to Build Flocs. Ph.D. thesis, Åbo Akademi University, Turku, Finland.

Bennington, C.P.J., Kerekes, R.J., Grace, J.R., 1990. The yield stress of fibre suspensions. Can J. Chem. Eng. 68, 748–757.

Bossis, G., Brady, J.F., 1987. Self-diffusion of Brownian particles in concentrated suspensions under shear. J. Chem. Phys. 9, 5437–5448.

Chaouche, M., Koch, D.L., 2001. Rheology of non-Brownian rigid fiber suspensions with adhesive contacts. J. Rheol. 45, 369–382.

Claeys, I.L., Brady, J.F., 1993a. Suspensions of prolate spheroids in Stokes flow. Part 1. Dynamics of a finite number of particles in an unbounded fluid. J. Fluid Mech. 251, 411–442.

Claeys, I.L., Brady, J.F., 1993b. Suspensions of prolate spheroids in Stokes flow. Part 2. Statistically homogeneous dispersions. J. Fluid Mech. 251, 443–477.

Fan, X.J., Phan-Thien, N., Zheng, R., 1998. A direct simulation of fibre suspensions. J. Non-Newton. Fluid Mech. 74, 113–135.

Farnood, R.R., Loewen, S.R., Dodson, C.T.J., 1994. Estimation of intra-floc forces. Appita 47, 391–396.

Harlen, O.G., Sundararajakumar, R.R., Koch, D.L., 1999. Numerical simulations of a sphere settling through a suspension of neutrally buoyant fibres. J. Fluid Mech. 388, 355–388.

Hourani, M.J., 1988. Fiber flocculation in pulp suspension flow, Part 2: Experimental results. Tappi J. 71, 186–189.

Kerekes, R.J., 1995. Perspectives on fibre flocculation in papermaking. In: Proceedings of the International Paper Physics Conference, Niagara-on-the-Lake, Ontario, September 1995. Canadian Pulp and Paper Association, Montreal, pp. 23–31.

Kerekes, R.J., Schell, C.J., 1992. Characterization of fibre flocculation regimes by a crowding factor. J. Pulp Pap. Sci. 18, J32–J38.

Kerekes, R.J., Schell, C.J., 1995. Effects of fiber length and coarseness on pulp flocculation. Tappi J. 78, 133–139.

Kerekes, R.J., Soszynski, R.M., Tam Doo, P.A., 1985. Transactions of the Eighth Fundamental Research Symposium, Oxford, vol. 1, pp. 265–310.

Mackaplow, M.B., Shaqfeh, E.S.G., 1996. A numerical study of the rheological properties of suspensions of rigid, non-Brownian fibres. J. Fluid Mech. 329, 155–186.
Mason, S.G., 1948. The flocculation of cellulose fibre suspensions. Pulp Paper Mag. Can. 49, 99–104.
Mason, S.G., 1950. The flocculation of pulp suspensions and the formation of paper. Tappi J. 33, 440–444.
Meyer, R., Wahren, D., 1964. On the elastic properties of three-dimensional fibre networks. Sven. Papperstidn. 67, 432–436.
Milliken, W.J., Gottlieb, M., Graham, A.L., Mondy, L.A., Powell, R.L., 1989. The viscosity volume fraction relation for suspensions of rod-like particles by falling ball rheometry. J. Fluid Mech. 202, 217–232.
Nilsen, N., Zabihian, M., Niskanen, K., 1998. KCL-PAKKA: a tool for simulating paper properties. Tappi J. 81, 163–166.
Robertson, A.A., 1956. The measurement of paper formation. Pulp Paper Mag. Can. 57, 119–127.
Ross, R.F., Klingenberg, D.J., 1997. Dynamic simulation of flexible fibers composed of linked rigid bodies. J. Chem. Phys. 106, 2949–2960.
Russel, W.B., Saville, D.A., Schowalter, W.R., 1989. Colloidal Dispersions. Cambridge University Press, Cambridge.
Schmid, C.F., 1999. Simulations of Flocculation in Flowing Fiber Suspensions. Ph.D. thesis, University of Wisconsin-Madison.
Schmid, C.F., Klingenberg, D.J., 2000a. Mechanical flocculation of flowing fiber suspensions. Phys. Rev. Lett. 84, 290–293.
Schmid, C.F., Klingenberg, D.J., 2000b. Properties of fiber flocs with frictional and attractive interfiber forces. J. Colloid Interface Sci. 226, 136–144.
Schmid, C.F., Switzer, L.H., Klingenberg, D.J., 2000. Simulations of fiber flocculation: effects of fiber properties and interfiber friction. J. Rheol. 44, 781–809.
Shchukin, E.D., Videnskii, I.V., Amelina, E.A., Bessonov, A.I., Parfenova, A.M., Aranovich, G., Donokhi, M., 1998. Adhesion of cellulose fibers in liquid media: 2. Measurement of contact force of attraction. Colloid J. 60, 541–543.
Soszynski, R.M., Kerekes, R.J., 1988a. Elastic interlocking of nylon fibers suspended in liquid. Part 1. Nature of cohesion among fibers. Nord. Pulp Paper Res. J. 3, 172–179.
Soszynski, R.M., Kerekes, R.J., 1988b. Elastic interlocking of nylon fibers suspended in liquid. Part 2. Process of interlocking. Nord Pulp Paper Res. J. 3, 180–184.
Sundararajakumar, R.R., Koch, D.L., 1997. Structure and properties of sheared fiber suspensions with mechanical contacts. J. Non-Newton. Fluid Mech. 73, 205–239.
Switzer III, L.H., 2002. Simulating Systems of Flexible Fibers. Ph.D. thesis, University of Wisconsin-Madison.
Switzer, L.H., Klingenberg, D.J., 2003. Rheology of sheared flexible fiber suspensions via fiber-level simulations. J. Rheol. 47, 759–778.
Takeuchi, N., Senda, S., Namba, K., Kuwabara, G., 1983. Formation and destruction of fibre flocs in a flowing pulp suspension. Appita 37, 223–230.
Tam Doo, P.A., Kerekes, R.J., 1981. A method to measure wet fiber flexibility. Tappi J. 64, 113–116.
Thalén, N., Wahren, D., 1964. Shear modulus and ultimate shear strength of some paper pulp fibre networks. Sven. Papperstidn. 67, 259–264.
Wittenburg, J., 1977. Dynamics of Systems of Rigid Bodies. B.G. Teubner, Stuttgart.
Yamamoto, S., Matsuoka, T., 1993. A method for dynamic simulation of rigid and flexible fibers in a flow field. J. Chem. Phys. 98, 644–650.
Yamamoto, S., Matsuoka, T., 1994. Viscosity of dilute suspensions of rodlike particles: a numerical simulation method. J. Chem. Phys. 100, 3317–3324.
Yamane, Y., Kaneda, Y., Doi, M., 1994. Numerical simulation of semi-dilute suspensions of rodlike particles in shear flow. J. Non-Newton. Fluid Mech. 54, 405–421.
Zauscher, S., Klingenberg, D.J., 2001. Friction between cellulose surfaces measured with colloidal probe microscopy. Colloid Surf. A 178, 213–229.
Zauscher, S., Scott, C.T., Willet, J.L., 2000. Pulp extrusion for recycling wastepapers and paper mill sludges. Tappi J. 83, 62.
Zhao, R.H., Kerekes, R.J., 1993. The effect of suspending liquid viscosity on fiber flocculation. Tappi J. 76, 183–188.